Science of the Total Environment 956 (2024) 176419

Contents lists available at ScienceDirect

Science of the Total Environment

journal homepage: www.elsevier.com/locate/scitotenv

Spatial multi-criteria approaches for estimating geogenic radon hazard index

Iman Masoumi [c], Sabrina Maggio [a], Sandra De Iaco [a,b,c,*], Reza Ghezelbash [d]

[a] Department of Economic Sciences, University of Salento, Lecce, Italy
[b] National Centre for HPC, Big Data and Quantum Computing, Bologna, Italy
[c] National Biodiversity Future Center, Palermo, Italy
[d] School of Mining Engineering, College of Engineering, University of Tehran, Tehran, Iran

HIGHLIGHTS

- The geogenic radon hazard index (GRHI) map allows evaluating radon exposure risks.
- The spatial multi-criteria decision analysis is proposed.
- Fuzzy gamma operator and AHP-TOPSIS for GRHI mapping.
- The success-rate curve is employed for the performance assessment.

GRAPHICAL ABSTRACT

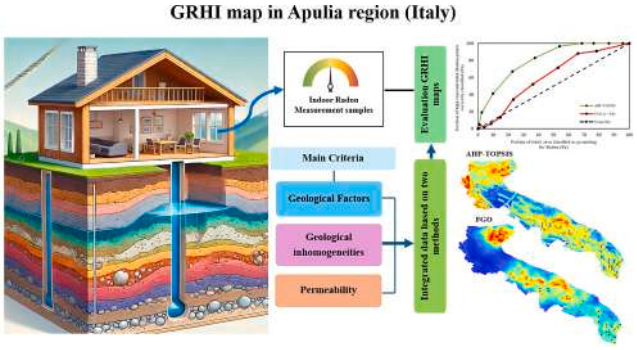

ARTICLE INFO

Editor: Pavlos Kassomenos

Keywords:
Radon risk
Fuzzy Gamma Operator (FGO)
Analytical Hierarchy Process (AHP)
TOPSIS
Multi-criteria analysis

ABSTRACT

The geogenic radon hazard index (GRHI) map plays a crucial role in evaluating radon exposure risks. The construction of this map requires a comprehensive analysis of radon levels in soil gas and some critical factors, such as uranium content in bedrock, soil permeability, and geological inhomogeneities. In this context, the spatial multi-criteria decision analysis is proposed with the aim of combining various key geological parameters and identifying high-potential radon areas. In particular, the multivariate integration involves the fuzzy gamma operator method and a hybrid multi-criteria decision-making technique, namely AHP-TOPSIS, which represents a novel approach in GRHI mapping. Thus, a comparison is provided through the definition of the GRHI maps of an unexplored study area, that is the Apulia region, located in Southern Italy. In order to evaluate the output maps, high radon potential areas are identified based on some available indoor radon measurement data. The success-rate curve, as a valid evaluation metric, is employed for the performance assessment and comparison of these two methods. The results demonstrate that although both generated GRHI maps are closely correlated with high-potential radon zones, the hybrid AHP-TOPSIS method is preferable.

* Corresponding author at: Department of Economic Sciences, University of Salento, Lecce, Italy.
E-mail address: sandra.deiaco@unisalento.it (S. De Iaco).

https://doi.org/10.1016/j.scitotenv.2024.176419
Received 19 July 2024; Received in revised form 29 August 2024; Accepted 18 September 2024
Available online 19 September 2024
0048-9697/© 2024 The Authors. Published by Elsevier B.V. This is an open access article under the CC BY-NC-ND license (http://creativecommons.org/licenses/by-nc-nd/4.0/).

1. Introduction

Studying radon and mapping the geogenic radon hazard are crucial due to the significant public health risk posed by indoor radon exposure (Angell, 2009). Second only to smoking, radon is a significant contributor to lung cancer, making it imperative to understand its relevant sources and pathways (UNSCEAR, 1982). In this regard, the GRHI map plays a significant role by providing a comprehensive view of the susceptibility of different areas to indoor radon concentration increase. A GRHI map is created by analyzing geogenic variables, such as geological maps and uranium content in bedrock and soil, in addition to other important variables like faults, karst features, and soil properties. This map helps policymakers and researchers in efficiently allocating resources in order to develop radon mitigation strategies (Cinelli et al., 2019; Bossew et al., 2020). Thus, it serves as a valuable tool, guiding efforts to prioritize areas where interventions are urgently needed to reduce radon exposure and mitigate its associated health risks. The construction of a GRHI map is also strategic in order to counteract the loss of biodiversity, which may cause serious consequences for the sustainability of the ecosystem and for human well-being.

Different methods can be applied with the aim to produce a GRHI map, each offering distinctive insights into radon hazards (Kemski et al., 2001; Gruber et al., 2013; Friedmann et al., 2017; Bossew et al., 2020; Petermann and Bossew, 2021). These methods are either data-driven or knowledge-driven. Advanced data-driven techniques include multivariate linear regression (Kropat et al., 2017), general linear models, and machine learning algorithms (Kropat et al., 2015; Timkova et al., 2017; Janik et al., 2018; Petermann et al., 2021; Al-Shboul et al., 2023), where geogenic quantities, such as geochemical concentration and soil properties are considered. This geogenic approach entails creating a weighted average of predictors. The weights can be implicit in cases of bivariate or multivariate scoring, where categorical predictor levels are assigned to GRHI levels based on experiential knowledge about their impact (Bossew et al., 2020). Alternatively, weights can be determined through correlation coefficients between predictors by utilizing techniques such as principal component analysis (PCA), hierarchical analysis and spatial multi-criteria decision analysis (SMCDA). These approaches guarantee a comprehensive assessment of radon hazards by considering various geological and environmental factors in a scientific context.

Only a few studies have explored the generation of GRHI map by recalling the SMCDA methods (Guida et al., 2013; Masoumi et al., 2024). To our knowledge, there is a noticeable absence of contributions focused on a combination of the hybrid FGO and multi-criteria decision making (MCDM) techniques, such as AHP-TOPSIS method, particularly in order to identify high-potential radon areas. Indeed, fuzzy approach provides a flexible framework for modeling vague information, hence for allowing the representation of complex relationships between input variables and results. By employing fuzzy sets and membership functions, this approach accommodates the inherent ambiguity in spatial data and expert knowledge, enhancing the robustness of hazard assessments. SMCDM methodologies offer systematic procedures for evaluating alternatives based on multiple conflicting criteria. In the case of mapping high-potential radon areas, SMCDM techniques, like AHP and TOPSIS, enable the integration of diverse factors such as geological, geophysical, and demographic data and provide a comprehensive assessment of radon hazard (Al Mohamed et al., 2023; Chakraborty et al., 2023). Consequently, this research aims at providing some advances in the construction of a comprehensive integrated model to effectively assess high-potential radon areas using FGO and hybrid AHP-TOPSIS techniques. For this reason, some available data in the Apulia region (Italy) have been used and a comparison of the effectiveness of these two methods in generating a GRHI map of the Apulia region has been proposed.

It is worth pointing out that generating a GRHI map in a given area is based on several crucial criteria, whose relevant layers must be combined. Therefore, the procedure can be regarded as an SMCDA method comprising three main steps: (1) collecting spatial data from multiple sources, (2) weighting the input layers, and (3) integrating the spatial dataset with the assigned weight values. Thus, the initial step of this analysis has involved the preprocessing of the collected layers of data, which have been transformed into the [0–1] domain through the fuzzy logic functions. The FGO model has been subsequently generated by integrating the fuzzified values. The integration has been achieved via different γ values, and the best value ($\gamma = 0.9$) has been chosen based on the Receiver Operating Characteristic (ROC) curve. Following this, the Natural Break method has been utilized to discretize the continuous values of some factors. This method has been regarded as a reliable classification technique and has been employed to categorize each evidential layer. By means of pairwise comparisons, meaningful weights have been subsequently assigned to the discretized classes; thus, this step has been conducted by recalling the AHP technique, known as one of the most prevalent methods in MCDM. The final step has been to compile all determined weights for each sub-criteria into a decision matrix with the scope of generating the GRHI map through the hybrid AHP-TOPSIS procedure. The obtained results have been evaluated and compared using the success-rate curve, which is a validation metric method (Parsa et al., 2016) based on the known area of high radon potential in the Apulia region. These areas have been identified using the method described in Cinelli et al. (2011) for indoor radon data. The findings indicate that, although the GRHI maps derived from the two different methods (FGO and AHP-TOPSIS) are in good agreement with the high-potential radon area in the Apulia region, the hybrid AHP-TOPSIS method shows a higher level of success in identifying areas with high radon potential.

It is worth pointing out that the implementation of AHP-TOPSIS procedure for radon risk mapping as well as the interest in producing a GRHI map for an unexplored area, such ar the Apulia region in Italy, represent the elements of novelty of this contribution. Indeed, the aim of this study is to propose a comprehensive and integrated innovative approach for constructing a GRHI map specifically for the Apulia region in Southern Italy. The study seeks to improve the identification of high-potential radon areas by employing advanced spatial multi-criteria decision-making techniques, particularly the hybrid AHP-TOPSIS method and FGO model. By comparing the effectiveness of these methods, this enhanced mapping tool not only deepens the understanding of radon distribution but also provides policymakers with a powerful resource for prioritizing radon mitigation efforts, ultimately contributing to the protection of public health in regions susceptible to elevated radon levels.

The remainder of the paper is organized as follows. In Section 2, a brief description of the study area as well as the presentation of the FGO method and the AHP-TOPSIS technique have been given. In Section 3, the data and the corresponding layers referred to the geological features useful to assess the high-potential radon areas have been illustrated. In Section 4, the GRHI maps for the Apulia region have been produced on the basis of the FGO and AHP-TOPSIS methods, then a comparative analysis based on the ROC curves has been proposed. Some conclusions have been provided in Section 5.

2. Materials and methods

The study process involves four main steps as described in Fig. 1: defining criteria and sub-criteria (Step 1), calculating significant weights using the AHP method (Step 2), integrating weighted spatial evidence layers and depicting target areas through the TOPSIS, while applying the fuzzy gamma method separately (Step 3), and comparing and evaluating the results (Step 4).

All data have been initially processed using the QGIS software within the geographic information system (GIS) environment and the final GRHI prospectivity mapping have been carried out in MATLAB software.

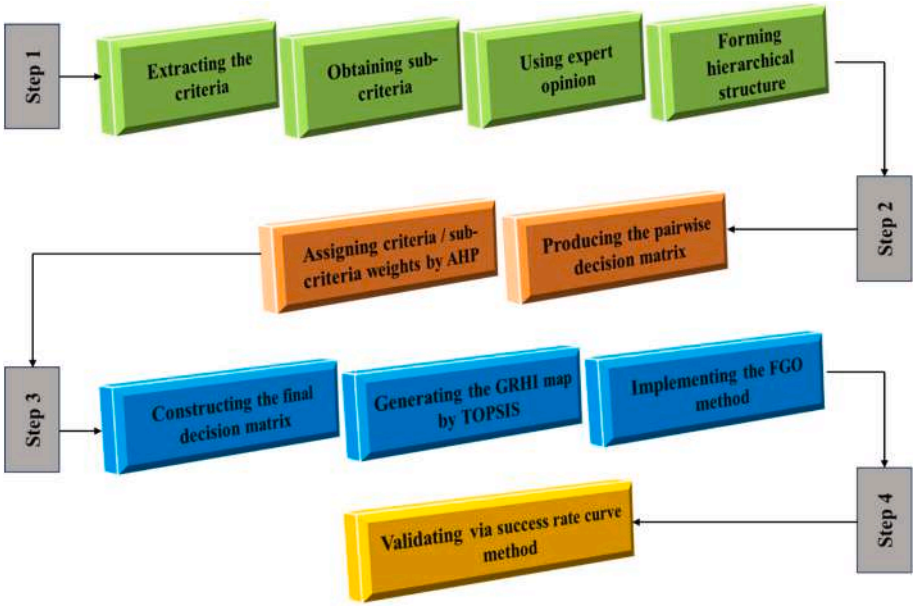

Fig. 1. Main steps and sub-steps to generate GRHI maps by using FGO and AHP-TOPSIS methods.

2.1. Geology of the study area

The area of interest, referred to the Apulia Region in Southern Italy, is an intriguing area for geological study. Fig. 2 depicts the geographical location of the domain and the primary lithology, including faults, caves, dolines, and sinkholes. Shaped by diverse geological phenomena, it is predominantly composed of Mesozoic carbonates and limestone rocks, especially in the central part of the region. The Southern and

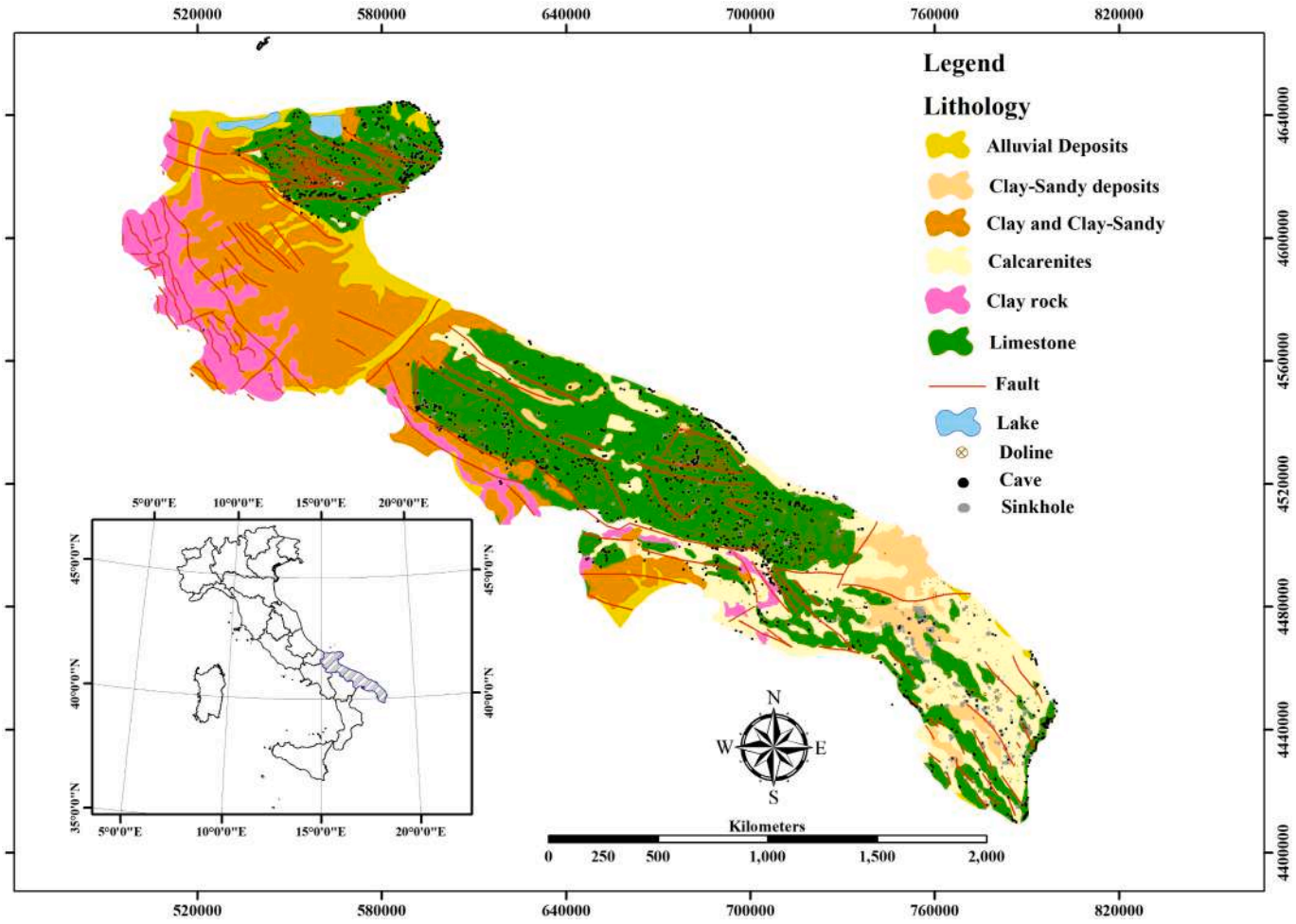

Fig. 2. Location of the study areas in Italy and geological map (Viel et al., 1986).

Northern parts are characterized by calcarenite and clay sandy rocks from the Cenozoic era, respectively. The limestone rocks in Apulia display minimal deformation, featuring broad, gentle folds occasionally interrupted by extensional faults. These limestone formations developed mainly during the Middle and Lower Jurassic periods, coinciding with the break-up of the supercontinent Pangaea. This geological activity resulted in the formation of gulfs and seas in areas that were previously terrestrial. Notably, this geological feature encompasses the Murge plateau, Gargano massif, and Salento Peninsula, collectively referred to as the Apulian Foreland. Extensive outcrops of these carbonates are also found in this region (De Santis and Caldara, 2015).

The region's tectonic framework is defined by pervasive NW-SE normal faulting and jointing, with an additional EW system of transitional areas, indicating a complex geological history (Tozzi et al., 1988). This tectonic diversity is further exemplified by the presence of high-angle faults, shaping the landscape and influencing the geological formations (Doglioni et al., 1994). Furthermore, Apulia is home to a variety of geological phenomena, with sinkholes being particularly noteworthy, as they have significantly influenced the evolution of the region's topography. These sinkholes result from karst processes whereby carbonate rocks are dissolved due to the aggressive interaction between saltwater from the sea and fresh groundwater (Cigna and Forti, 1986). Sinkholes often manifest as abrupt collapses, which change the topography and contribute to the unique geological identity of Apulia (Johnson, 1989).

In Section 3, a detailed description of the data and the corresponding layers is given.

2.2. FGO method

The concept of fuzzy logic, initially introduced by Zadeh (1965), finds widespread applications in integrating spatial evidence layers with fuzzy information. This integration involves the definition of weights for the data, which can be based on expert judgments. To standardize input values, fuzzy member weights are calculated, and continuous values ranging from 0 to 1 are assigned to relevant pixels in exploration evidence layers. Fuzzy logic employs five fuzzy operators: gamma, algebraic SUM, AND, OR, and algebraic PRODUCT. However, the OR and AND operators, commonly used with fuzzy membership functions, have limitations. The OR operator yields the maximum output value, whereas the AND operator provides the minimum value. Fuzzy algebraic PRODUCT, fuzzy algebraic SUM, and FGO are employed to combine data in order to circumvent these limitations (Bonham-Carter, 1994). In this approach, outputs are determined as follows:

$$\mu_p(x) = \prod_{i=1}^{n} \mu_i(x) \tag{1}$$

$$\mu_s(x) = 1 - \left(\prod_{i=1}^{n} 1 - \mu_i(x) \right) \tag{2}$$

where n denotes the number of membership functions to be merged, and μ_i represents the i^{th} membership function. The fuzzy algebraic product function produces an outcome equal to or smaller than the minimum of the provided function. In contrast, the fuzzy algebraic sum function yields results that surpass all inputs but never exceed 1. FGO is calculated using the equation given below:

$$\mu_\gamma(x) = [\mu_s(x)]^\gamma \times \left[\mu_p(x)\right]^{1-\gamma} \tag{3}$$

where γ-value must be within the [0–1] range to optimize the membership fusion (Zimmermann and Zysno, 1980). When γ is established at 1, the fusion resembles the fuzzy algebraic SUM. On the other hand, a γ value of 0 results in fusion akin to the fuzzy algebraic PRODUCT. By selecting an appropriate γ, output values can balance the effects of the fuzzy algebraic PRODUCT and the fuzzy algebraic SUM (Ying, 2003). Thus, the Gamma operator effectively combines the fuzzy algebraic PRODUCT and fuzzy algebraic SUM operators, resulting in reliable output values by mitigating the exaggerated impact of the fuzzy algebraic SUM while compensating for the diminishing impact of the fuzzy algebraic PRODUCT (Akbari et al., 2020).

2.3. The hybrid AHP-TOPSIS procedure

The AHP, introduced by Saaty (1977), stands for Analytical Hierarchy Process and is a widely used MCDM method applied extensively in various fields such as engineering, industry and management (Chan and Kumar, 2007; Lima Junior et al., 2014; Greco et al., 2016; Zhang et al., 2015; Akbari et al., 2020). AHP addresses complex decision-making challenges by breaking them down into hierarchies of interconnected decision elements. It facilitates the prioritization of influential criteria by evaluating the significance of distinct criteria and their sub-criteria via pairwise comparisons.

The TOPSIS method, another significant MCDM technique, was initially introduced by Hwang and Yoon (1981) and later enhanced by Chen and Hwang (1992). This method aims to ascertain the optimal option from a limited set of alternatives. TOPSIS is based on the principle of finding the option that comes closest to the positive ideal solution, which maximizes benefit and minimizes cost criteria. Conversely, the negative ideal solution aims at minimizing benefit criteria while maximizing cost criteria. Decision-makers utilize TOPSIS by selecting an alternative that is closest to the positive ideal solution and farthest from the negative ideal solution, a concept introduced by Abo-Sinna and Amer (2005) and further detailed by Jahanshahloo et al. (2006) and Shih et al. (2007). This fundamental idea underpins the TOPSIS method, enabling effective decision-making by striking a balance between benefits and costs.

A hybrid MCDM approach has been employed in this study by integrating the AHP and TOPSIS techniques that draws upon various MCDM methods applied in previous research (Tavana and Hatami-Marbini, 2011; Abedi and Norouzi, 2016; Akbari et al., 2020; Nazim et al., 2022; Singh et al., 2023). Through this integrated approach, the decision-making process is optimized, ensuring a comprehensive evaluation of the alternatives based on both benefit and cost considerations. This algorithm has been used to rank and assign the weights to distinct criteria related to high radon concentrations.

In AHP, the objectives and alternatives are systematically compared to determine the relative importance of the alternatives. Saaty's nine-point scale (Saaty, 1977) is used to compare the significance of objectives, as shown in Table 1. The eigenvector method is applied to calculate the weights and assess the consistency of the weights obtained

Table 1
Scale of pairwise comparison in AHP method.

Criteria intensity	Description	Intensity degree of importance
1	The two criteria have an identical objective.	Equal
3	A factor is prioritized marginally against another.	Moderate
5	A criterion is highly prioritized against another.	Strong
7	One criterion is given significantly higher priority over another, and this is clearly demonstrated through actions.	Very strong
9	The proof for prioritizing one criterion over another has the highest possible strength to validate.	Extreme
2, 4, 6, 8	Deployed to show the comprises between the preference scores 1, 3, 5, 7, and 9.	Intermediate value between two adjacent judgments
Reciprocity	Deployed to do inverse comparisons.	Opposites

through pairwise comparisons. The Consistency Ratio (CR) is used to ensure that the results are consistent. To be considered consistent, the CR must not exceed 0.10 or 10% (Saaty, 1977).

Then, in the context of solving multi-criteria problems, AHP and TOPSIS are integrated for decision-making purposes. The process is detailed as follows (Pazand et al., 2012; Menon and Ravi, 2022; Hsu et al., 2008):

Step 1. A decision matrix consisting of criteria and attributes is created through pairwise comparisons. This matrix is given below:

$$C = \begin{bmatrix} c_{11} & \cdots & c_{1n} \\ \vdots & \ddots & \vdots \\ c_{n1} & \cdots & c_{nn} \end{bmatrix} = \begin{array}{c} \\ C_1 \\ C_2 \\ \vdots \\ C_n \end{array} \begin{array}{c} \begin{array}{cccc} C_1 & C_2 & \cdots & C_n \end{array} \\ \begin{bmatrix} 1 & a_{12} & \cdots & a_{1n} \\ 1/a_{12} & 1 & \cdots & a_{2n} \\ \vdots & \vdots & \ddots & \vdots \\ 1/a_{1n} & 1/a_{2n} & \cdots & 1 \end{bmatrix} \end{array}, \tag{4}$$

where c_{ij} represents the relative significance of the i^{th} attribute compared to the j^{th} attribute as regards the overall objective. Alternatively, given the set of criteria and sub-criteria $C_1, C_2, \ldots, C_n$, the pairwise comparison matrix C can be defined through the coefficient a_{ij} which represents the judgment according to the scale described in Table 1. The outcomes of comparing the criteria and sub-criteria are incorporated into the upper triangular of the pairwise comparison matrix C. The lower triangular values represent the relative positions corresponding to the reciprocal values of the upper triangular matrix. Specifically, for a given pair of criteria or sub-criteria (C_i, C_j), with $i, j = 1, 2, \ldots, n$, $i \neq j$, the single value a_{ij} is provided, then the relative judgment for the inverse comparison (C_j, C_i) becomes $a_{ji} = 1/a_{ij}$.

Step 2. The decision matrix is normalized using the following equation:

$$m_{ij} = \frac{c_{ij}}{\sum_{i=1}^{n} c_{ij}} \tag{5}$$

Step 3. The weights for criteria and sub-criteria are normalized and the check on consistency is provided. Thus, the vector of the weights is denoted with

$$W = [w_i]_{n\times 1} \tag{6}$$

and its elements w_i are normalized as follows:

$$w_i = \sum_{j=1}^{n} \frac{m_{ij}}{n}, i = 1, 2, \ldots, n. \tag{7}$$

Then, the largest eigenvalue λ_{max} is computed from the matrix C, so that it is employed to assess the consistency index (CI) and consistency ratio (CR) of the comparison matrix, as defined below:

$$CI = \frac{\lambda_{max} - n}{n - 1} \tag{8}$$

$$CR = \frac{CI}{RI} \tag{9}$$

where RI is the random consistency index, which serves as a measure of the average randomness in the ranking of attributes based on various pairwise comparisons. In Table 2 the RI values for different values of n are shown. If the computed CR is equal to or <10% (0.10), it indicates that the assessment of attribute importance is reliable, and any inconsistencies can be disregarded. On the other hand, a CR value >10% suggests that the comparisons lack of consistency, necessitating corrections to the judgments in the matrix.

Step 4. A matrix X which accounts for attributes measured in different units, is normalized. This transformation converts the matrix into dimensionless units, allowing for comparisons across criteria. The data are normalized in the following manner:

$$r_{ij} = \frac{x_{ij}}{\left(\sum_{i=1}^{n} x_{ij}^2\right)^{0.5}}, i = 1, 2, \ldots, n \text{ and } j = 1, 2, \ldots, m, \tag{10}$$

in which x_{ij} denotes the element of the decisional matrix X, where j represents the alternatives (pixel values of evidence layers) and i denotes the criteria.

Step 5. The elements v_{ij} of the weighted normalized matrix V are calculated according to the following equation:

$$v_{ij} = w_i r_{ij}, i = 1, 2, \ldots, n \text{ and } j = 1, 2, \ldots, m. \tag{11}$$

Note that w_i, i=1,2,...,n, represent the computed weights to be assigned to the criteria, such as those determined through the AHP.

Step 6. The positive ideal solution is presumed to possess superior beneficial characteristics and minimal costs (A^+), while the negative ideal solution is assumed to have the least favorable attributes in terms of benefits and the highest costs (A^-). The subsequent expression provides a definition for A^+ and A^-.

$$A^+ = \left\{ max\left(v_{ij} | j \in J\right) min\left(v_{ij} | j \in J'\right) \right\} = \left\{ v_1^+, \ldots., v_n^+ \right\} \tag{12}$$

$$A^- = \left\{ min\left(v_{ij} | j \in J\right) max\left(v_{ij} | j \in J'\right) \right\} = \left\{ v_1^-, \ldots., v_n^- \right\} \tag{13}$$

where J is related to the beneficial attributes or equivalently positive criteria, and J' is related to the non-beneficial attributes or equivalently negative criteria (Ghezelbash et al., 2024).

Step 7. The separation measures, denoted as $D_i = \left\{S_i^+, S_i^-\right\}$ are calculated using the Euclidean distance as follows:

$$S_i^+ = \sqrt{\sum_{j=1}^{n} \left(v_{ij} - v_j^+\right)^2}, i = 1, \ldots, m, \tag{14}$$

$$S_i^- = \sqrt{\sum_{j=1}^{n} \left(v_{ij} - v_j^-\right)^2}, i = 1, \ldots, m. \tag{15}$$

Note that S_i^+ represents the separation of each alternative from the positive ideal solution (superior beneficial characteristics and minimal costs) and S_i^- represents the separation of each alternative from the negative ideal solution (minimum beneficial characteristics and maximum costs).

Step 8. The relative proximity of alternatives to the ideal solution is calculated as follows:

$$DD_i^+ = \frac{S_i^-}{S_i^+ + S_i^-}, i = 1, \ldots, m, \tag{16}$$

Table 2
Values for the random consistency index RI, given the matrix order n (Saaty and Vargas, 2013)

n	1	2	3	4	5	6	7	8	9	10
RI	0	0	0.53	0.9	1.12	1.24	1.32	1.41	1.45	1.49

given $S_i^+ + S_i^- > 0$, then it results that $DD_i^+ \in [0,1]$. A high relative closeness value indicates a more favorable alternative.

Step 9. The assessment of a set of options is subsequently established based on the comparative proximity values DD_i^+.

3. Data used and evidence layer preparation

The GRHI serves as a fundamental tool in the scientific evaluation of indoor radon concentration risks, addressing both natural and anthropogenic determinants (Sakoda et al., 2011). Geogenic factors, which are inherent to the earth's geology, involve complex processes of radon generation and subsurface transport. These processes depend on geological, soil, and hydrological parameters. Such factors exhibit discernible geographical patterns and spatial structures, reflecting the nuanced interplay of geological elements influencing radon exposure risks (Bossew et al., 2020; Ciotoli et al., 2007).

Key geological parameters, notably the concentration of uranium in rocks and soils, soil permeability, and geological inhomogeneities, play a central role in the GRHI framework. These geological attributes, compounded by climatic variations, exert substantial influence on radon levels in soil gas (Cinelli et al., 2019). The GRHI, quantified on a dedicated scale, integrates these multifaceted factors, enabling a comprehensive analysis of potential radon exposure risks in specific locations or areas. It is necessary to consider and incorporate the above-mentioned factors, systematically in the assessment process. The crucial criteria and their corresponding sub-criteria, as well as their references for introducing the GRHI map using the MCDM method, are provided in Table 3 and described in the subsequent section.

3.1. Uranium concentration in rocks and soils

The uranium concentration in soils and rocks is crucial for evaluating radon (^{222}Rn) exposure risk (Matolín, 2017). Uranium-238 (^{238}U) is naturally found in various rocks, ranging from low levels in sedimentary rocks to high levels in magmatic rocks (Smethurst et al., 2017). The content of uranium in soil can be calculated via geochemical or radiological analysis methods. Radiological analysis involves direct measurement of uranium using alpha spectrometry or indirect measurement through its progenies, (like ^{214}Bi and ^{214}Pb) using gamma spectrometry. European soil geochemical data, gathered extensively, offer valuable regional insights. This study utilized uranium, thorium, and potassium concentration maps from the European Atlas of Natural Radiation, created by using data from the Geochemical Atlas of Europe and Geochemical Mapping of Agricultural and Grazing Land Soil projects. These maps, accessible at a 10 km × 10 km resolution, have been collected from the Joint Research Centre data catalogue at https://data.jrc.ec.europa.eu/dataset and used for analysis. Furthermore, according to Nogarotto (2018) and the results of uranium content mapping in Italy's bedrock, the large part of the involved area in the Apulia region has been categorized into three different lithological types based on the lithological units: Late Cretaceous-Paleogene sedimentary rocks, Eocene-Oligocene-Miocene sedimentary rocks, and Mesozoic carbonate rocks. These categories have been associated with high, medium, and low uranium content in bedrock, respectively. The Euclidean distance algorithm has been used in the QGIS software to comprehensively cover the entire Apulia region and investigate the effects of three specific layers on radon concentration in various parts of the region, as well as to create final GRHI maps (Dokmanic et al., 2015). In Fig. 3(a to f), the maps on the left display the uranium content in bedrock and soil in the Apulia region.

3.2. Geological inhomogeneities

Geological and human-made factors significantly influence radon concentration in soil gas at specific locations (Ciotoli et al., 2016; Cinelli et al., 2019). These factors include permeable irregularities, subvertical orientations, intersections with various rock types, and the presence of faults. Faults, notable geological irregularities, play a crucial role in radon movement in soil. Their placement in regions with active or passive geodynamic activity, proximity to the fault plane, and the type of bedrock govern radon velocity and concentration in shallow soils. Radon anomalies above faults vary in intensity and spatial distribution due to factors such as sediment layers, aquifers, and fault geometry. The development of fault zones and fractures is closely associated with radon anomaly distribution. Fault cores act as radon pathways, while surrounding damage zones release radon, especially when the core is impermeable. Regions with high levels of fracturing, cracking, and lithological variations exhibit varying permeability levels and radon concentration changes (Annunziatellis et al., 2008; Pereira et al., 2010; Seminsky et al., 2014; Ciotoli et al., 2016). In karstic regions, radon flow depends on convective features within the karstic bedrock, including caves, sinkholes, and dolines, which contribute significantly to radon transport. Faults, caves, dolines, and sinkholes have been identified as significant contributors in various studies (Petermann and Bossew, 2021; Coletti et al., 2022).

Researchers have emphasized the importance of fault characteristics, particularly proximity to faults when studying radon concentration. High radon emissions are observed in highly faulted areas, indicating that proximity to faults leads to higher radon concentrations. Soil permeability, which in turn affects radon gas concentrations, varies according to the distribution of rocks and the severity of faulting and fractures. Rock fractures and faults beneath the surface offer high permeability paths, enabling radon gas migration. Therefore, the presence of faults contributes to elevated radon concentrations in soil. Dwellings located closer to faults are more likely to exceed radon guidelines, increasing vulnerability to elevated indoor radon levels. The presence of geological faults near dwellings provides favorable pathways for radon migration from uranium-rich bedrock units to the

Table 3
Primary criteria and sub-criteria considered for the GRHI map.

Source of radon in soil gas	Primary criteria	Sub-criteria	References
Geological factor	Uranium concentration in rocks and soils	Uranium, thorium, and potassium concentrations in soil	https://data.jrc.ec.europa.eu/dataset
		Uranium content in bedrock	(Nogarotto, 2018)
	Geological Inhomogeneities	Fault	https://www.isprambiente.gov.it/it, http://www.sit.puglia.it
		Cave	
		Doline	
		Sinkhole	
	Permeability	Fine fraction	https://esdac.jrc.ec.europa.eu/content/topsoil-physical-properties-europe-based-lucas-topsoil-data
		Bulk Density	
		Available Water Capacity (AWC)	
		Texture	

surface, resulting in elevated indoor radon levels (Amponsah et al., 2008; Drolet and Martel, 2016).

In this study, the distance to the fault has been calculated and considered as an input layer for processing. The information regarding different layers in the Apulia region has been sourced from the ISPRA (Higher Institute for Environmental Protection and Research) and SIT Puglia website (http://www.sit.puglia.it). The Euclidean distance algorithm (Dokmanic et al., 2015) has been used in QGIS software to generate maps illustrating the distances to faults, dolines, caves, and sinkholes, as depicted in the left maps in Fig. 3(g to j).

3.3. Permeability

Soil gas radon concentrations are highly dependent on permeability, which measures the geological environment's capacity to transport soil gases such as radon from their source (weathered or solid rock) to the surface or inhabited areas (Nazaroff, 1992). Various factors such as soil texture, temperature, pressure fluctuations, and soil moisture influence this transportation rate. Radon is released into empty spaces from mineral grains containing uranium in the soil. The movement of radon relies on the interconnectedness of these spaces, enabling both vertical and horizontal motion. However, vertical movement might be limited by specific mineral particles or clay layers in the soil. The European soil erodibility map was established using parameters like soil organic

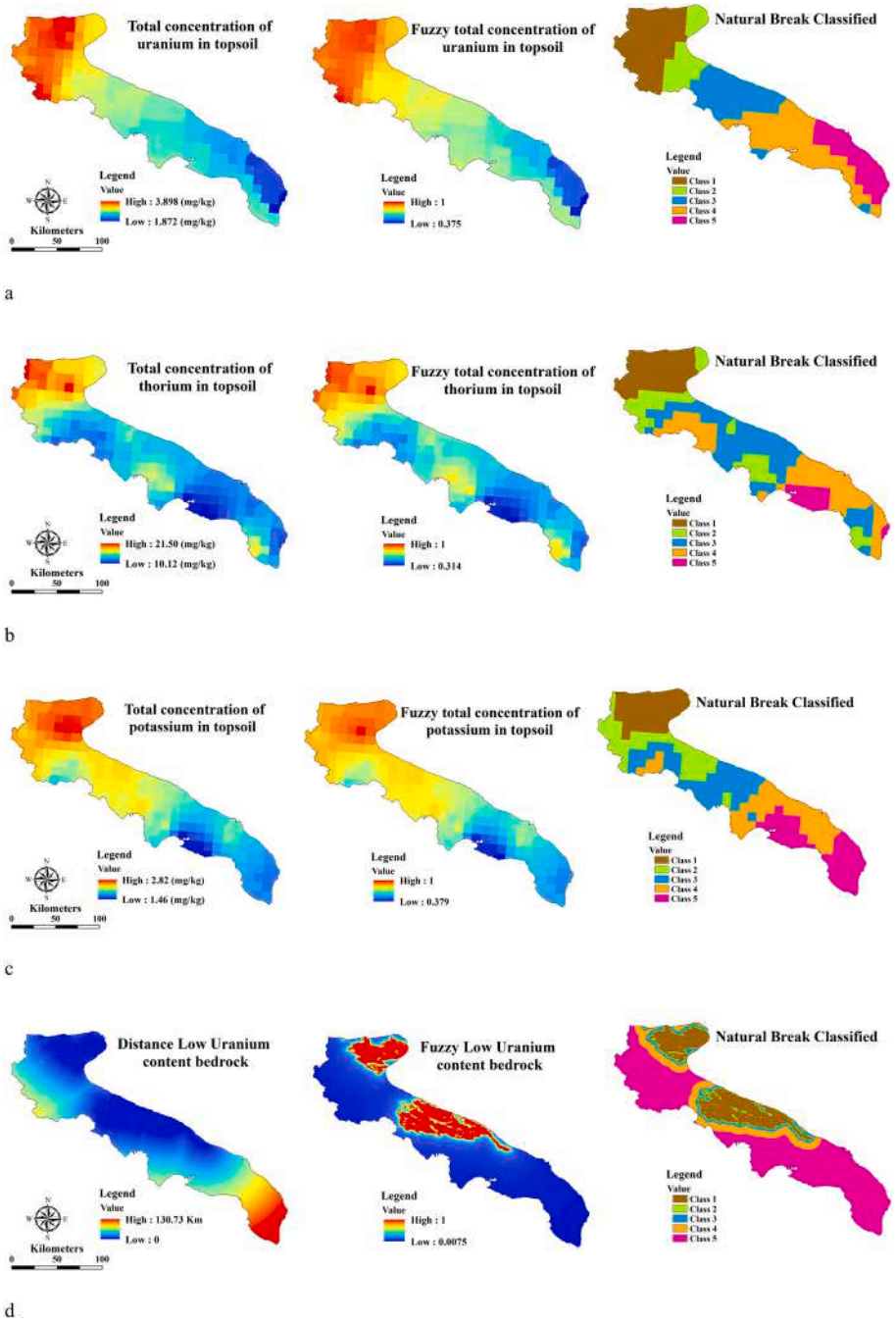

Fig. 3. Various elements pertaining to geological factors and assessments, delineating (a to f) for uranium concentration in bedrock and soil, (g to j) for geological inhomogeneities (e.g., faults, dolines, caves, sinkholes), and (k to n) for permeability layers (e.g., texture, AWC, bulk density, fine fraction). Each row illustrates the sequence: raw data (left map), fuzzified layer (center map), and final classified map (right map).

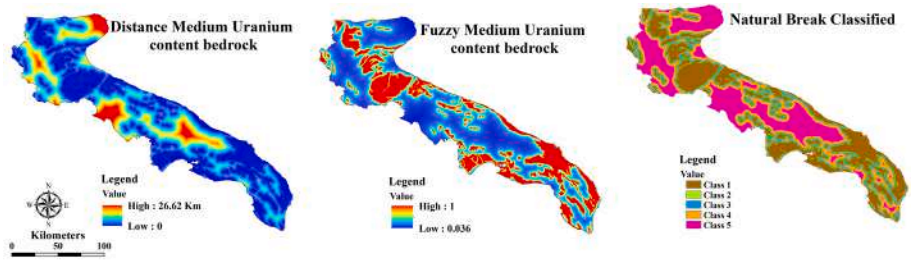

e

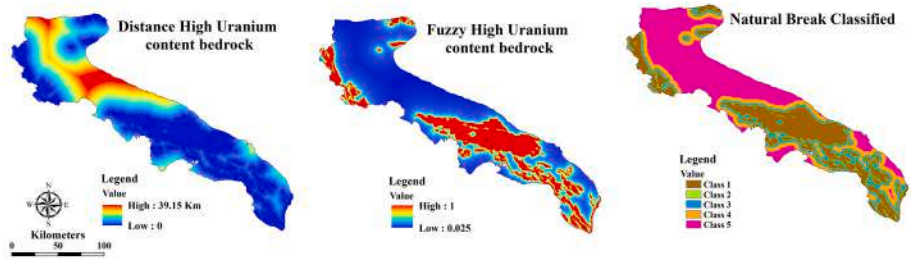

f

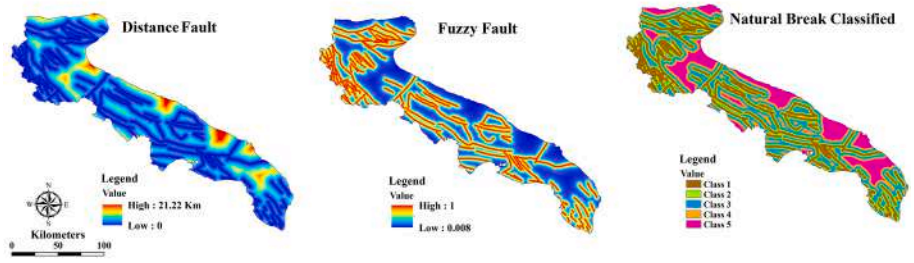

g

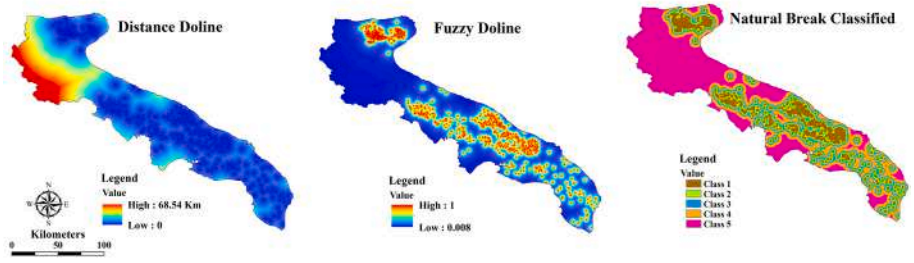

h

Fig. 3. (*continued*).

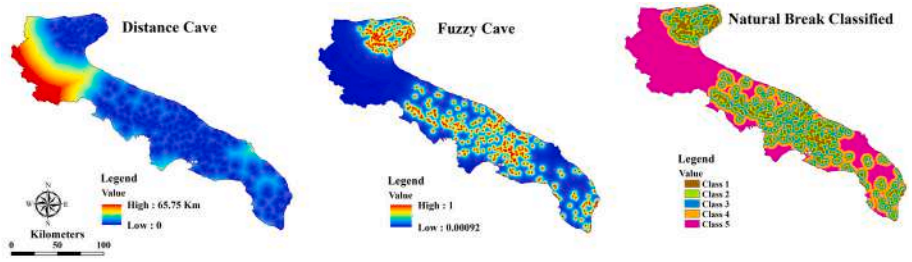

i

j

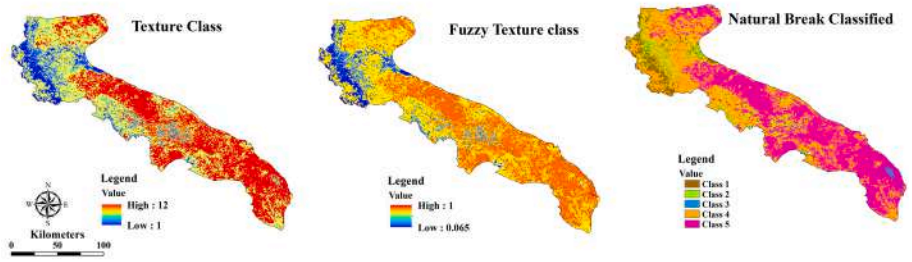

k

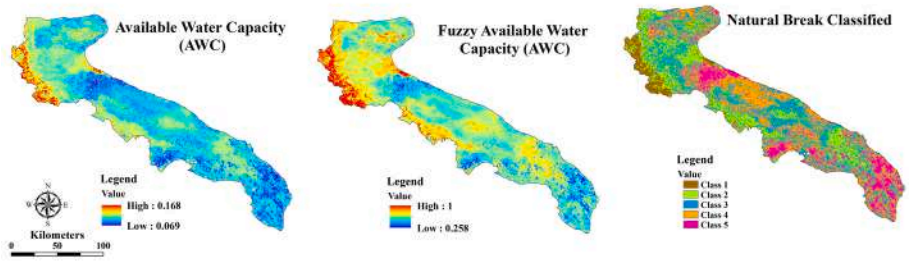

l

Fig. 3. (*continued*).

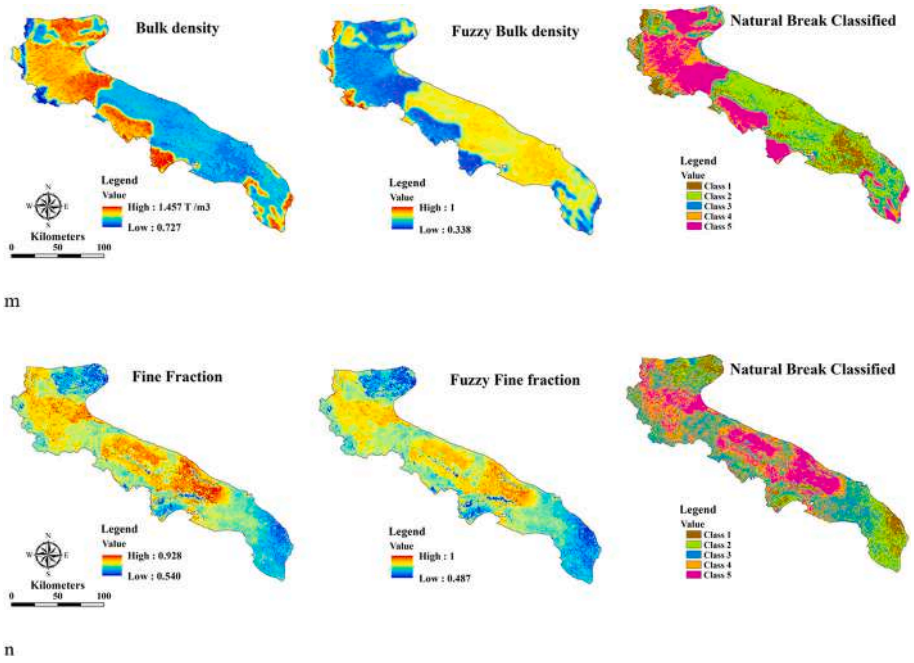

Fig. 3. (*continued*).

carbon, soil texture (sand, silt, clay), permeability, soil structure, stone cover, and coarse fragments from the LUCAS database (Land Use/Cover Area frame Statistical Survey). Soil permeability estimates were based on textural classes since European-scale specific data were lacking. Further analyses were introduced and improvement was achieved by integrating data on the fraction of ultra-fine sand and hydraulic conductivity, resulting in more precise estimates of soil erodibility and permeability (Cinelli et al., 2019). Panagos et al. (2014) focused on analyzing the physical properties of topsoil in Europe using data from the LUCAS topsoil dataset. The finalized maps containing this information can be accessed at European Soil Data Center (Panagos et al., 2012, 2022). The study encompassed the following details:

(1) Multivariate Additive Regression Splines were used to model the percentages of silt, clay, sand, and coarse fragments in the topsoil.

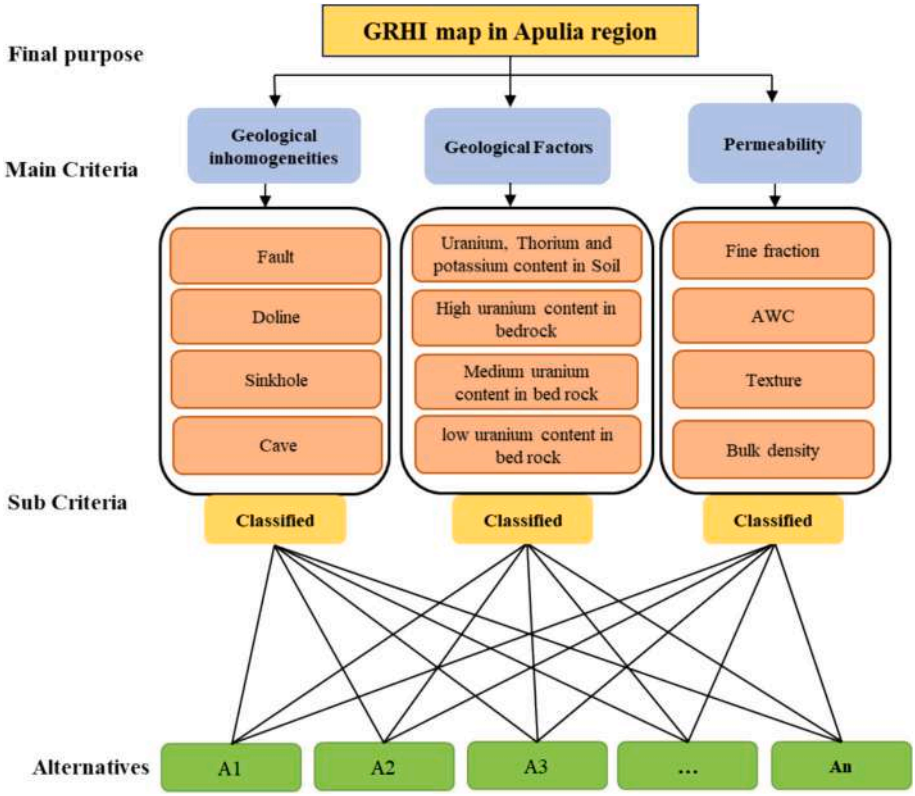

Fig. 4. Criteria hierarchy model for Apulia GRHI map.

(2) Bulk density values were calculated using soil texture datasets calculated based on (Ballabio et al., 2016).
(3) USDA soil textural classes were determined based on silt, clay, and sand maps.
(4) AWC for the fine earth fraction in the topsoil was assessed.

In this research, the fine fraction of soil has been calculated using LUCAS texture maps, which offer comprehensive information about soil properties throughout Europe. The maps on the left in Fig. 3 (k to n) illustrate the conclusive maps within the Apulia region of AWC, bulk density, soil texture, and the fine fraction.

3.4. Fuzzification and classification of layers

Before integrating the geospatial layers derived from available data in this region, it is crucial to normalize their values within a consistent range. This normalization is necessary because the minimum and maximum values in each layer is not uniform. For this purpose, fuzzy member functions can be used to convert the continuous-value pixels of the evidential layers into a fuzzy space. This allows for the representation of values within the [0–1] range. In this study, the small and large fuzzy membership functions commonly utilized in geoscience fields, have been used to convert the values of different layers into the [0–1] range using QGIS software. The small fuzzy membership function is used when smaller input values provide more significance, resulting in higher membership values (Raines et al., 2010). This function highlights the probability of incorporating smaller input values into the set; thus, values below the midpoint receive increased emphasis.

The large fuzzy function, introduced by Mohebbi Tafreshi et al. (2021) and Raines et al. (2010), is utilized for emphasizing large input values; as a consequence, values exceeding the midpoint are highly likely to be part of the set, whereas values below the midpoint have a lower probability of being included. This function enhances membership values above the midpoint, leading to greater fitness. Eqs. (17) and (18), formally defines the small and large membership functions:

$$\mu(x) = \frac{1}{1 + \left(\frac{x}{f_2}\right)^{f_1}} \tag{17}$$

$$\mu(x) = \frac{1}{1 + \left(\frac{x}{f_2}\right)^{-f_1}} \tag{18}$$

where $\mu(x)$ represents the membership value of the category, while f_1 and f_2 denote the spread and midpoint values, respectively. The final fuzzy maps of the input layers are shown in the center of Fig. 3.

The Natural Breaks method is a statistical classification technique commonly used in QGIS. This has been employed in this study to partition a dataset into distinct and internally homogeneous classes. This is achieved by minimizing the variance within each class and maximizing the variance between classes. By grouping similar data values together, this method ensures that there is minimal difference within each class and a significant difference between classes (Jenks and Caspall, 1971; Baz et al., 2009). The Natural Break method is used to classify the input data into five classes, which are shown in the right maps of Fig. 3.

Finally, the criteria hierarchy model useful to introduce the Apulia GRHI map is shown in Fig. 4.

Table 4
Pairwise comparison between Natural Break classes of three criteria and 14 sub-criteria and their allocated weights using AHP.

Criteria	Weight	Sub-critical	Weight	Classes	Weight	Criteria	Weight	Sub-critical	Weight	Classes	Weight
Geological factors (uranium concentration in rocks and soil)	0.311	Uranium in soil	0.158	1	0.033	Permeability	0.196	Fine fraction	0.041	1	0.033
				2	0.017					2	0.017
				3	0.008					3	0.009
				4	0.004					4	0.004
				5	0.002					5	0.002
		Thorium in soil	0.041	1	0.009			Bulk Density	0.083	1	0.060
				2	0.004					2	0.031
				3	0.002					3	0.015
				4	0.001					4	0.007
				5	0.003					5	0.004
		Potassium in soil	0.013	1	0.003			Texture	0.069	1	0.055
				2	0.001					2	0.028
				3	0.001					3	0.016
				4	0.0005					4	0.006
				5	0.0005					5	0.003
		High Uranium in bedrock	0.148	1	0.062	Geological inhomogeneities	0.493	Fault	0.141	1	0.141
				2	0.029					2	0.084
				3	0.016					3	0.031
				4	0.006					4	0.014
				5	0.003					5	0.008
		Medium uranium in bedrock	0.050	1	0.021			Cave	0.071	1	0.024
				2	0.009					2	0.014
				3	0.005					3	0.005
				4	0.002					4	0.003
				5	0.001					5	0.001
		Low uranium in bedrock	0.014	1	0.006			Sinkhole	0.071	1	0.024
				2	0.003					2	0.013
				3	0.001					3	0.003
				4	0.0005					4	0.002
				5	0.0005					5	0.001
Permeability	0.196	AWC	0.029	1	0.021			Doline	0.071	1	0.024
				2	0.011					2	0.014
				3	0.005					3	0.005
				4	0.003					4	0.002
				5	0.001					5	0.001

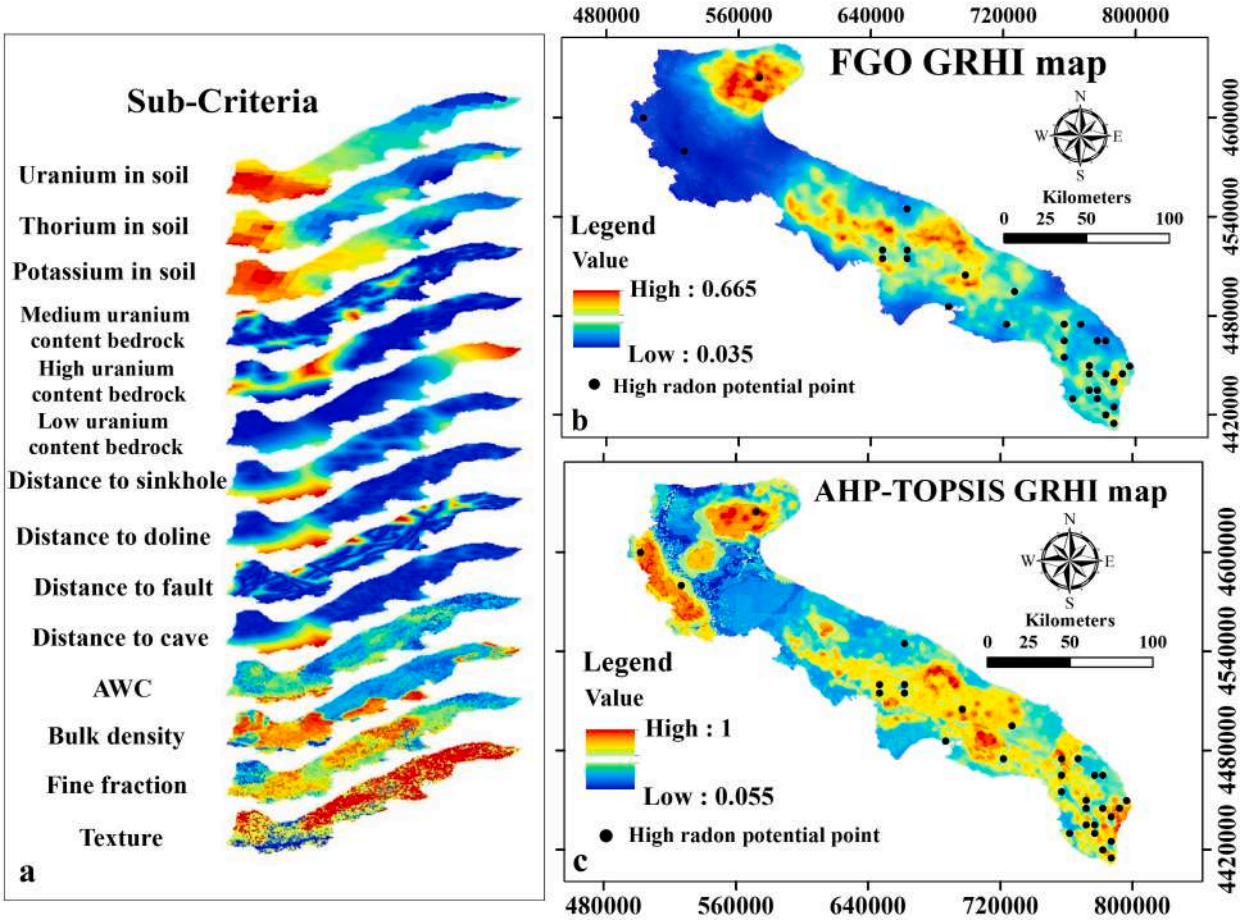

Fig. 5. a) 14 different sub-criteria used for generating GRHI map, b) the final GRHI map based on FGO method, c) final GRHI map based on AHP-TOPSIS method.

3.5. Allocating competent weights to the criteria and sub-criteria

The assessment of the relative importance of different evidence layers and their competent weights is a crucial and challenging issue. Assigning these weights should be carried out by genuine experts who possess ample knowledge about the radon issue and the dataset collected in the examined area.

As illustrated in Fig. 4, the primary focus of this study is to generate GRHI map in Apulia region on the basis of three main factors, including uranium content, geological inhomogeneities, and permeability, which are segmented into 14 sub-criteria. These sub-criteria take into account the scores that have been assigned to prioritize these criteria based on inputs gathered from various expert opinions and a comprehensive review of articles and technical documents related to the subject (Ciotoli et al., 2017; De Iaco et al., 2017; Coletti et al., 2022). Additionally, a pairwise comparison matrix has been created for the elements within each hierarchical level, guided by the expertise of decision-makers. The matrix has been employed to compute the final weights for each criterion, sub-criterion, and their respective classes, as outlined in Table 4.

4. Mapping GRHI in Apulia region

Two approaches, FGO and AHP-TOPSIS, have been utilized to construct a GRHI map and then the results have been compared through the success-rate curves.

4.1. FGO model

The fuzzy logic overlay method has been recalled to integrate criteria into a single GRHI map. Initially, the values of 14 sub-criteria have been transformed into a [0–1] range based on eqs. (17) and (18). These transformed values have served as weighted fuzzy evidence layers, allowing the application of various fuzzy operators such as fuzzy AND, OR, SUM, Gamma, and PRODUCT operators so as to synthesize these layers, as described in Bonham-Carter (1994). The FGO has been particularly advantageous in comparison to fuzzy SUM and fuzzy PRODUCT operators due to its ability to counteract the “decrease” effect of the fuzzy PRODUCT operator and the “increase” effect of the fuzzy SUM operator, as in Yousefi and Carranza (2015).

In this study, the continuous-value multidisciplinary evidence layers (layers with fuzzy membership values), have been integrated in order to compute fuzzy prospectivity scores for identifying areas with high radon potential. An optimal γ value has been selected using eq. (3) among different values, and the best one has been chosen by applying the ROC curve, as described in Section 4.3.2. Consequently, a fuzzy-based GRHI map has been generated to delineate promising areas associated with the high potential of radon in the Apulia region (Fig. 5).

4.2. Hybrid AHP-TOPSIS model

This research aims to integrate various layers so as to identify areas with high radon potential in an unexplored study region (Apulia region - Italy). For this purpose, the study innovatively employs the AHP-TOPSIS procedure, a hybrid MCDM procedure that comprises AHP and TOPSIS techniques. Indeed, the AHP has been used to calculate the competent weights of criteria, sub-criteria, and alternatives, while the TOPSIS has been utilized to integrate different evidence layers and to rank the pixel scores.

The approach consists of three main phases: (a) establishing the basic criteria and their corresponding sub-criteria and classes in accordance

with the study's main aim; (b) calculating substantial weights (Table 4) and applying them to criteria, sub-criteria and their relevant classes using the AHP method; and (c) integrating and ranking different levels of weighted evidence using the TOPSIS framework. In the initial phase, pertinent data concerning key factors linked to the study's objective has been gathered. Subsequently, a hierarchical structure has been designed, as depicted in Fig. 4. The MCDM problem can be decomposed, using the AHP method, into interconnected components, namely criteria and sub-criteria.

The hierarchical framework comprises three primary levels: (a) the highest tier introduces the Apulia region's GRHI map, which is the central focus of this study; (b) the intermediate level encompasses the main criteria, including geological factors, geological inhomogeneities and permeability. These criteria have been further delineated into 14 fuzzified and classified sub-criteria; (c) the lowest tier accommodates the decision alternatives. Specifically, the pixel values from integration layers, which are associated with high radon potential, have served as the basis for defining the alternatives and ranking according to the TOPSIS method.

Next, a decision matrix has been constructed to allocate significant weights to the criteria, sub-criteria, and alternatives. This matrix has been established via pairwise comparisons, utilizing expert opinions and the scale provided by Saaty (1977) in Table 3. Subsequently, significant weights for each criterion and its associated classes have been calculated and assigned using the AHP method. These calculated weights are presented in Table 4, demonstrating the comprehensive evaluation of the hierarchical structure in this study. As depicted in this table, geological inhomogeneities emerged as the most influential factor, possessing a weight of 0.493. The geological factor and permeability, with weights of 0.311 and 0.196 respectively, indicate their significance. Similarly, various sub-criteria and Natural Break classes associated with each criterion underwent weighting through the AHP, whose outcomes are presented in Table 4.

In the third step, the primary objective is to identify prospective areas with high radon potential in the Apulia region using weighted criteria and sub-criteria. In order to accomplish this objective, a decision matrix has been generated, wherein the pixel values extracted from 14 fuzzified maps and represented as alternatives have been denoted by the horizontal rows, and the 14 sub-criteria have been located in the vertical columns. The initial matrix used to implement the AHP-TOPSIS procedure comprised a total of 77,184 rows and 14 columns. Following that, a MATLAB-based program has been executed to weigh and rank the multidimensional alternatives using the AHP-TOPSIS approach. This process has led to the generation of a high-potential radon model. A visual examination of the results reveals a positive spatial correlation between known high radon potential areas and the high prospective scores on the prospectivity map (Fig. 5).

4.3. Assessment of the GRHI maps in the Apulia region

The efficiency of GRHI maps is evaluated using the success-rate curves method. As illustrated below, this approach is based on the known presence of high-potential radon concentration and the areas occupied by various anomaly classes in the evidence layers.

4.3.1. High-potential radon concentration in the Apulia region

To identify areas with high radon potential in the Apulia region, this study has analyzed 2018 samples of radon measurement data obtained from the Apulia Regional Environmental Protection Agency in Italy. The samples have been collected from indoor environments across the Apulia region, and refer to different ground and underground levels of dwellings, schools, and workplaces in combination with other information about building and ground characteristics. Sampled data were taken by using SSNTD (NRPB/SSI type passive dosimeters) with six-month exposure periods. Quality control included calibration with certified radon atmospheres and adherence to ISO 17025 standards, ensuring reliable results. The objective of identifying areas with high radon potential has been pursued through a systematic analysis that is enumerated below:

(1) According to Cinelli et al. (2011), a correction coefficient of 0.82 is applied to underground (basement) data to convert them into ground data.
(2) According to Article 103 of Directive 2013/59/EURATOM (BSS), the reference level for identifying high radon areas, based on percentage sampling measurements exceeding 300 Bq/m^3, is established at 15%.
(3) The region is divided into cells, each covering an area of one square kilometer. Geological information is linked and considered to the central point of each cell.
(4) For each cell, the logarithmic mean radon concentration is calculated and compared to the corresponding value of the smoothed logarithmic mean.
(5) The percentage above the action level (P) for each cell is calculated using the following equation:

$$P = \int_{5.1}^{\infty} exp\left(-\frac{(x - lm)^2}{2\sigma_G^2} \right) \cdot \frac{1}{\sigma_G \sqrt{2\pi}} dx \cdot 100 \quad (19)$$

where x represents the natural logarithm of radon concentration and lm represents the logarithm mean computed for the cell, while σ_G is the standard deviation of the logarithmic values for the particular geological group/cell. The threshold level, fixed at 5.1 and equivalent to logarithm of 300 Bq/m^3, indicates the action level. Thus, the check that the percentage sampling measurements exceeding 300 Bq/m^3, denoted with P, is >15% has been conducted.

(6) High-potential points associated with its cells are mapped (Cinelli et al., 2011).

In Fig. 5, the high potential areas recognized in this method are shown as black points in the final GRHI maps.

4.3.2. Validation of FGO maps by the ROC curve

The FGO maps of areas with high radon potential have been generated for γ values of 0.80, 0.85, 0.90, and 0.95. Next, these maps have been validated based on the existing areas with high radon potential, which were defined in the previous step. A ROC curve is an analytical technique, as explained in Giglioni et al. (2021) and Nahm (2022), which provides a graphical tool for quantifying the performance of a

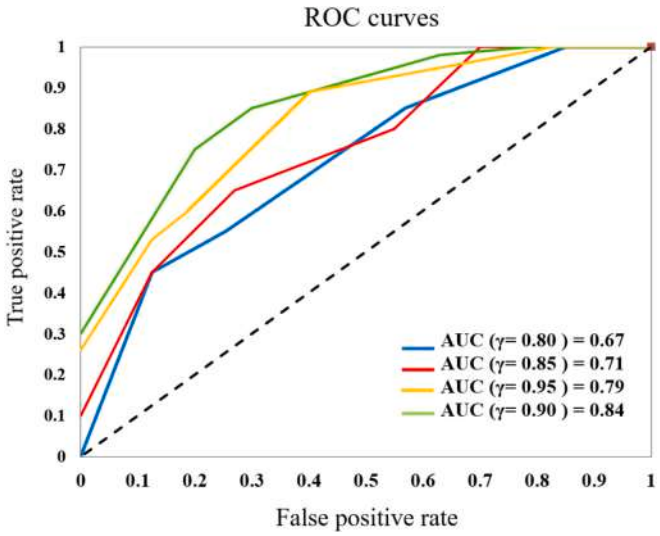

Fig. 6. Evaluation of the ROC curves for different γ values.

process. The following confusion matrix D is fundamental for evaluating the performance of classifiers and computing the integral of the ROC curves:

$$D = \begin{bmatrix} TP & FP \\ FN & TN \end{bmatrix} \tag{20}$$

where

- *TP* stands for True Positive, that is correctly identified positive instances
- *FP* stands for False Positive, that is instances incorrectly classified as positive
- *TN* stands for True Negative, that is correctly identified negative instances
- *FN* stands for False Negative, that is instances incorrectly classified as negative

Thus, the true positive rate (*TPr*), also referred to as sensitivity or the probability of detection, quantifies the proportion of accurately identified positive instances among all actual positive samples; conversely, the false positive rate (*FPr*), also known as the probability of false alarms, indicates the proportion of incorrectly identified positive instances among all actual negative samples:

$$TPr = \frac{TP}{TP + FN} \tag{21}$$

$$FPr = \frac{FP}{FP + TN} \tag{22}$$

The ROC curve can be constructed by plotting the *TPr* against the *FPr* for different threshold values. It should be noted that as the curve approaches the upper left corner of the ROC space, the model's accuracy increases, but the model's accuracy decreases as the curve approaches the 45-degree diagonal line in the ROC space.

The reliability of the ROC curve is calculated on the basis of the AUC values (0 to 1), which correspond to the area under the curve, that is,

$$\mathrm{AUC} = \int_0^1 ROC(f)df \tag{23}$$

where *f* is associated to the *FPr*, while *ROC(f)* denotes the corresponding *TPr*. If the model fails to identify a radon hazard area, the AUC becomes equal to or lower than 0.5. The AUC value ranging from 0.5 to 1 indicates the performance of a model, with higher values suggesting better discrimination between two classes, as highlighted by Fawcett (2006) and Nahm (2022).

Fig. 6 depicts the ROC curves, drawn for various γ values. Then, the AUC values of 0.67, 0.71, 0.84, and 0.79 correspond to γ values of 0.80, 0.85, 0.90, and 0.95, respectively. Notably a γ value of 0.90 yields the highest AUC value and has been chosen for the final FGO map.

4.3.3. Evaluation of final GRHI maps using the success-rate curve method

This study employs an improved success-rate curve approach to evaluate the effectiveness of GRHI maps. The constructed success-rate curve illustrates the accurately categorized portion of the study area (Pa) along the horizontal axis and the portion of the target associated with high radon potential (Po) within the study area along the vertical axis. In order to assess the importance and effectiveness of prospectivity maps the gauge line, which is a diagonal line, is drawn. Positive spatial associations can be determined by comparing the relevant success-rate curve with the gauge line. If the curve is above the gauge line, it indicates a positive association between the prospectivity map and its corresponding targets, meaning that map is able to precisely predict the desired targets. Conversely, if the curve is below the gauge line, it suggests a lack of positive spatial association (Carranza and Laborte, 2015; Parsa et al., 2016; Ghezelbash and Maghsoudi, 2018). For comparative purposes, it is crucial to display all success-rate curves within the same plot. When the success-rate curve of a prospectivity map exceeds another, it suggests a stronger spatial correlation with high radon concentration.

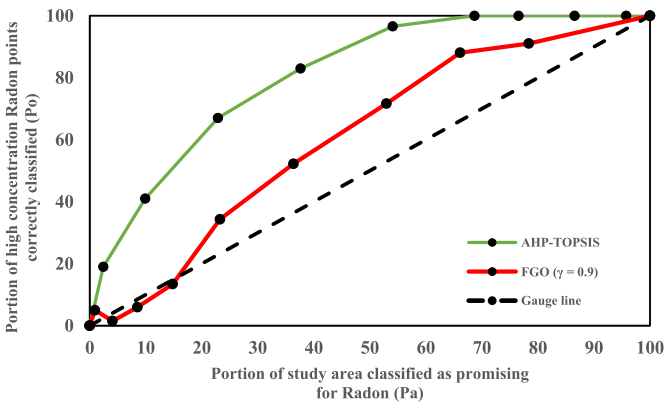

Fig. 7. Success rate curves for two GRHI mapping models.

This study has employed success-rate curves to compare and evaluate two prospectivity models namely hybrid AHP-TOPSIS and FGO. The Pa and Po values for the two GRHI maps have been calculated using a 10-percentile interval. This has been done to quantitatively evaluate and compare the AHP-TOPSIS and FGO (with $\gamma = 0.9$) GRHI maps. Fig. 7 shows the success-rate curves for the hybrid AHP-TOPSIS and FGO models.

The analysis of Fig. 7 reveals that both prospectivity models effectively delineate promising areas with high potential radon, as their success-rate curves are above the gauge line. Nonetheless, the success-rate curve of the former model surpasses the gauge line to a greater extent compared to the latter model, indicating a higher level of success in identifying areas with elevated radon potential. Note that the final GRHI map, which integrates geogenic factors like uranium content in bedrock, soil permeability and geological inhomogeneities, shows a strong correlation with high indoor radon levels in the Apulia region. The validation, using success rate curves and ROC analysis, confirms the effectiveness of the model in predicting radon prone areas.

The AHP-TOPSIS model primarily focuses on geogenic factors, which are crucial indicators of radon potential in dwellings. However, it is worth recognizing that building-related variables, such as construction materials, foundation integrity, and ventilation, also significantly influence indoor radon concentrations. This complexity means that while the geogenic-based predictions are robust, variations in indoor radon levels can sometimes occur due to these additional factors.

This consideration further explains why, in some cases, the predicted radon-prone areas may not perfectly correspond to high indoor radon levels. However, despite these further challenges, the proposed model effectively identifies areas with elevated radon risk, as demonstrated by the validation results.

5. Conclusion

Given the significance of identifying high-potential radon areas and the complexity involved in achieving this goal using various criteria, the construction of a GRHI map for a specific region necessitates the use of multidisciplinary spatial datasets from various sources related to geogenic factors and radon transportation.

In this study, a novel approach, called AHP-TOPSIS, was introduced for combining specific characteristics of the recognized high-potential radon zones and expert opinions. Thus, for the first time, a GRHI map for the Apulia region (in Southern Italy) was created using this method. 3 primary factors and 14 sub-criteria were identified and represented as spatial layers, that serve as effective indicators of radon high potential.

To standardize the data, the fuzzification functions were applied, and consistent scale layers were produced. Subsequently, the Natural Break method was employed to classify and discretize the fuzzified values from the 14 evidence layers. Hence, the AHP was employed to allocate significant weights to different layers of evidence and interconnected distinct populations. This allowed for identifying regions that have a high likelihood of radon contamination. In order to evaluate this approach, a FGO map was performed, excluding any expert opinions and relying solely on fuzzified values from continuous evidential layers. Finally, a conceptual validation model was implemented using success-rate curves. This approach was employed to quantitatively assess the GRHI maps.

The success rate curves for the two different methods of GRHI mapping (AHP-TOPSIS and FGO) are positioned significantly above the diagonal line. This suggests that both models align well with the known high-potential areas of radon. However, the outcomes from the hybrid AHP-TOPSIS approach have proved to be more impactful when contrasted with the FGO method. Consequently, the application of this novel approach for GRHI mapping in the Apulia region not only have produced the first GRHI map, but have also demonstrated its effectiveness, as an MCDM method, for such mapping. This finding substantiates the viability of the proposed method for future applications in GRHI mapping. Moreover, based on the results on the elevated radon potential areas identified through this approach, policymakers and researchers can be empowered to adopt appropriate actions in order to effectively reduce radon exposure and its associated health risks.

As a further development, supplementary data regarding information about building and ground characteristics can be also included and studied even through other approached including artificial neural networks.

CRediT authorship contribution statement

Iman Masoumi: Writing – review & editing, Writing – original draft, Software, Methodology, Investigation, Formal analysis, Data curation, Conceptualization. **Sabrina Maggio:** Writing – original draft, Visualization, Validation, Supervision, Investigation, Conceptualization, Writing – review & editing. **Sandra De Iaco:** Writing – review & editing, Writing – original draft, Supervision, Funding acquisition, Conceptualization. **Reza Ghezelbash:** Supervision.

Declaration of competing interest

The authors declare that they have no known competing financial interests or personal relationships that could have appeared to influence the work reported in this paper.

Data availability

Data will be made available on request.

Acknowledgements

This research was supported by the National Biodiversity Future Center-NBFC, Spoke 4, Activity 4.1, sub activity 4.1.1.

Funder

Project funded under the National Recovery and Resilience Plan (NRRP), Mission 4 Component 2 Investment 1.4 - Call for tender No. 3138 of 16 December 2021, rectified by Decree n.3175 of 18 December 2021 of Italian Ministry of University and Research funded by the European Union – Next GenerationEU.

Award Number: Project code CN_00000033, Concession Decree No. 1034 of 17 June 2022 adopted by the Italian Ministry of University and Research, CUP F87G22000290001, Project title “National Biodiversity Future Center - NBFC”.

We would like to thank the anonymous peer reviewers for their valuable feedbacks and constructive suggestions, which have significantly improved the quality of this manuscript. In addition, we extend our heartfelt gratitude to Dr. Giorgia Cinelli for invaluable assistance and guidance throughout the course of this project, which greatly enriched the study.

References

Abedi, M., Norouzi, G.-H., 2016. A general framework of TOPSIS method for integration of airborne geophysics, satellite imagery, geochemical and geological data. Int. J. Appl. Earth Obs. Geoinf. 46, 31–44.

Abo-Sinna, M.A., Amer, A.H., 2005. Extensions of TOPSIS for multi-objective large-scale nonlinear programming problems. Appl. Math. Comput. 162, 243–256.

Akbari, S., Ramazi, H., Ghezelbash, R., Maghsoudi, A., 2020. Geoelectrical integrated models for determining the geometry of karstic cavities in the Zarrinabad area, west of Iran: combination of fuzzy logic, C-A fractal model and hybrid AHP-TOPSIS procedure. Carbonates Evaporites 35, 56.

Al Mohamed, A.A., Al Mohamed, S., Zino, M., 2023. Application of fuzzy multicriteria decision-making model in selecting pandemic hospital site. Fut. Bus. J. 9, 14.

Al-Shboul, K.F., Almasabha, G., Shehadeh, A., Alshboul, O., 2023. Exploring the efficacy of machine learning models for predicting soil radon exhalation rates. Stoch. Env. Res. Risk A. 37, 4307–4321.

Amponsah, P., Banoeng-Yakubo, B., Andam, A., Asiedu, D., 2008. Soil radon concentration along fault systems in parts of south eastern Ghana. J. Afr. Earth Sci. 51, 39–48.

Angell, W.J., 2009. WHO Handbook on Indoor Radon: A Public Health Perspective. World Health Organization.

Annunziatellis, A., Beaubien, S.E., Bigi, S., Ciotoli, G., Coltella, M., Lombardi, S., 2008. Gas migration along fault systems and through the vadose zone in the Latera caldera (central Italy): implications for CO_2 geological storage. Int. J. Greenhouse Gas Control 2 (3), 353–372.

Ballabio, C., Panagos, P., Monatanarella, L., 2016. Mapping topsoil physical properties at European scale using the LUCAS database. Geoderma 261, 110–123.

Baz, I., Geymen, A., Er, S.N., 2009. Development and application of GIS-based analysis/synthesis modeling techniques for urban planning of Istanbul Metropolitan Area. Adv. Eng. Softw. 40, 128–140.

Bonham-Carter, G.F., 1994. Spatial Data Transformations (Chapter 6), Tools for Map Analysis: Multiple Maps (Chapter 9). In: Bonham-Carter, G.F. (Ed.), Geographic Information Systems for Geoscientists: Modelling with GIS. Pergamon. https://doi.org/10.1016/C2013-0-03864-9.

Bossew, P., Cinelli, G., Ciotoli, G., Crowley, Q.G., De Cort, M., Medina, J.E., Gruber, V., Petermann, E., Tollefsen, T., 2020. Development of a geogenic radon hazard index—concept, history, experiences. Int. J. Environ. Res. Public Health 17 (11), 4134.

Carranza, E.J.M., Laborte, A.G., 2015. Random forest predictive modeling of mineral prospectivity with small number of prospects and data with missing values in Abra (Philippines). Comput. Geosci. 74, 60–70. https://doi.org/10.1016/j.cageo.2014.10.004.

Chakraborty, S., Raut, R.D., Rofin, T.M., Chakraborty, S., 2023. A comprehensive and systematic review of multi-criteria decision-making methods and applications in healthcare. Healthc. Anal. 4, 100232.

Chan, F.T.S., Kumar, N., 2007. Global supplier development considering risk factors using fuzzy extended AHP-based approach. Omega (Westport) 35, 417–431.

Chen, S.J., Hwang, C.L., 1992. Fuzzy Multiple Attribute Decision Making Methods. In: Fuzzy Multiple Attribute Decision Making. In: Lecture Notes in Economics and Mathematical Systems. Springer, Berlin, Heidelberg, p. 375. https://doi.org/10.1007/978-3-642-46768-4_5. Methods and Applications.

Cigna, A., Forti, P., 1986. The speleogenetic role of air flow caused by convection. 1st contribution. Int. J. Speleol. 15, 41–52.

Cinelli, G., Tollefsen, T., Bossew, P., Gruber, V., Bogucarskis, K., De Felice, L., De Cort, M., 2019. Digital version of the European Atlas of natural radiation. J. Environ. Radioact. 196, 240–252. https://doi.org/10.1016/j.jenvrad.2018.02.008.

Cinelli, G., Tondeur, F., Dehandschutter, B., 2011. Development of an indoor radon risk map of the Walloon region of Belgium, integrating geological information. Environ. Earth Sci. 62, 809–819.

Ciotoli, G., Lombardi, S., Annunziatellis, A., 2007. Geostatistical analysis of soil gas data in a high seismic intermontane basin: Fucino Plain, central Italy. J. Geophys. Res. 112, B05407.

Ciotoli, G., Sciarra, A., Ruggiero, L., Annunziatellis, A., Bigi, S., 2016. Soil gas geochemical behaviour across buried and exposed faults during the 24 august 2016 central Italy earthquake. Ann. Geophys. 59. https://doi.org/10.4401/ag-7242.

Ciotoli, G., Voltaggio, M., Tuccimei, P., Soligo, M., Pasculli, A., Beaubien, S.E., Bigi, S., 2017. Geographically weighted regression and geostatistical techniques to construct the geogenic radon potential map of the Lazio region: a methodological proposal for the European Atlas of Natural Radiation. J. Environ. Radioact. 166, 355–375.

Coletti, C., Ciotoli, G., Benà, E., Brattich, E., Cinelli, G., Galgaro, A., Massironi, M., Mazzoli, C., Mostacci, D., Morozzi, P., Mozzi, P., Nava, J., Ruggiero, L., Sciarra, A., Tositti, L., Sassi, R., 2022. The assessment of local geological factors for the construction of a Geogenic Radon Potential map using regression kriging. A case study from the Euganean Hills volcanic district (Italy). Sci. Total Environ. 808, 152064.

De Iaco, S., Maggio, S., Palma, M., 2017. Radon predictions with geographical information system covariates: from spatial sampling to modeling. Geogr. Anal. 49, 215–235.
De Santis, V., Caldara, M., 2015. The 5.5–4.5 kyr climatic transition as recorded by the sedimentation pattern of coastal deposits of the Apulia region, southern Italy. Holocene 25 (8), 1313–1329.
Doglioni, C., Mongelli, F., Pieri, P., 1994. The Puglia uplift (SE Italy): an anomaly in the foreland of the Apenninic subduction due to buckling of a thick continental lithosphere. Tectonics 13, 1309–1321.
Dokmanic, I., Parhizkar, R., Ranieri, J., Vetterli, M., 2015. Euclidean distance matrices: essential theory, algorithms, and applications. IEEE Signal Process. Mag. 32, 12–30.
Drolet, J.-P., Martel, R., 2016. Distance to faults as a proxy for radon gas concentration in dwellings. J. Environ. Radioact. 152, 8–15.
Fawcett, T., 2006. An introduction to ROC analysis. Pattern Recogn. Lett. 27, 861–874.
Friedmann, H., Baumgartner, A., Bernreiter, M., Gräser, J., Gruber, V., Kabrt, F., Kaineder, H., Maringer, F.J., Ringer, W., Seidel, C., Wurm, G., 2017. Indoor radon, geogenic radon surrogates and geology – investigations on their correlation. J. Environ. Radioact. 166, 382–389.
Ghezelbash, S., Ghezelbash, R., Kalantari, M., 2024. Developing a spatio-temporal interactions model for car crashes using a novel data-driven AHP-TOPSIS. Appl. Geogr. 162, 103151.
Ghezelbash, R., Maghsoudi, A., 2018. Comparison of *U*-spatial statistics and C–A fractal models for delineating anomaly patterns of porphyry-type Cu geochemical signatures in the Varzaghan district, NW Iran. Comptes Rendus Géoscience 350 (4), 180–191. https://doi.org/10.1016/j.crte.2018.02.003.
Giglioni, V., García-Macías, E., Venanzi, I., Ierimonti, L., Ubertini, F., 2021. The use of receiver operating characteristic curves and precision-versus-recall curves as performance metrics in unsupervised structural damage classification under changing environment. Eng. Struct. 246, 113029. https://doi.org/10.1016/j.engstruct.2021.113029.
Greco, S., Ehrgott, M., Figueira, J.R. (Eds.), 2016. Multiple Criteria Decision Analysis. Springer, New York.
Gruber, V., Bossew, P., De Cort, M., Tollefsen, T., 2013. The European map of the geogenic radon potential. J. Radiol. Prot. 33, 51–60.
Guida, D., Guida, M., Cuomo, A., Guadagnuolo, D., Siervo, V., 2013. Assessment and Mapping of Radon-Prone Areas on a Regional Scale as Application of a Hierarchical Adaptive and Multi-Scale Approach for the Environmental Planning. Case Study of Campania Region. Southern Italy. WSEAS Trans. Syst. 12 (2), 105–120. https://wseas.com/journals/systems/2013/56-329.pdf.
Hsu, P.-F., Wu, C.-R., Li, Y.-T., 2008. Selection of infectious medical waste disposal firms by using the analytic hierarchy process and sensitivity analysis. Waste Manag. 28 (8), 1386–1394. https://doi.org/10.1016/j.wasman.2007.05.016.
Hwang, C.L., Yoon, K., 1981. Methods for Multiple Attribute Decision Making. In: Multiple Attribute Decision Making. In: Lecture Notes in Economics and Mathematical Systems, 186. Springer, Berlin, Heidelberg. https://doi.org/10.1007/978-3-642-48318-9_3.
Jahanshahloo, G.R., Lotfi, F.H., Izadikhah, M., 2006. Extension of the TOPSIS method for decision-making problems with fuzzy data. Appl. Math. Comput. 181, 1544–1551.
Janik, M., Bossew, P., Kurihara, O., 2018. Machine learning methods as a tool to analyse incomplete or irregularly sampled radon time series data. Sci. Total Environ. 630, 1155–1167.
Jenks, G.F., Caspall, F.C., 1971. Error on choroplethic maps: definition, measurement, reduction. Ann. Assoc. Am. Geogr. 61, 217–244.
Johnson, K.S., 1989. Development of the Wink Sink in west Texas, U.S.A., due to salt dissolution and collapse. Environ. Geol. Water Sci. 14, 81–92.
Kemski, J., Siehl, A., Stegemann, R., Valdivia-Manchego, M., 2001. Mapping the geogenic radon potential in Germany. Sci. Total Environ. 272, 217–230.
Kropat, G., Bochud, F., Jaboyedoff, M., Laedermann, J.-P., Murith, C., Palacios (Gruson), M., Baechler, S., 2015. Improved predictive mapping of indoor radon concentrations using ensemble regression trees based on automatic clustering of geological units. J. Environ. Radioact. 147, 51–62.
Kropat, G., Bochud, F., Murith, C., Palacios (Gruson), M., Baechler, S., 2017. Modeling of geogenic radon in Switzerland based on ordered logistic regression. J. Environ. Radioact. 166, 376–381.
Lima Junior, F.R., Osiro, L., Carpinetti, L.C.R., 2014. A comparison between Fuzzy AHP and Fuzzy TOPSIS methods to supplier selection. Appl. Soft Comput. 21, 194–209.
Masoumi, I., Maggio, S., De Iaco, S., 2024. An Advanced Spatial Approach Based on Multi-criteria Analysis and Geostatistical Simulation for a Comprehensive Geogenic Radon Hazard Index Mapping. J. Agr. Biol. Envir. St. https://doi.org/10.1007/s13253-024-00654-6.
Matolín, M., 2017. Verification of the radiometric map of the Czech Republic. J. Environ. Radioact. 166, 289–295.
Menon, R.R., Ravi, V., 2022. Using AHP-TOPSIS methodologies in the selection of sustainable suppliers in an electronics supply chain. Clean. Mater. 5, 100130.
Mohebbi Tafreshi, G., Nakhaei, M., Lak, R., 2021. Land subsidence risk assessment using GIS fuzzy logic spatial modeling in Varamin aquifer, Iran. GeoJournal 86 (3), 1203–1223.
Nahm, F.S., 2022. Receiver operating characteristic curve: overview and practical use for clinicians. Korean J. Anesthesiol. 75 (1), 25–36.
Nazaroff, W.W., 1992. Radon transport from soil to air. Rev. Geophys. 30 (2), 137–160.
Nazim, Mohd, Wali Mohammad, C., Sadiq, Mohd., 2022. A comparison between fuzzy AHP and fuzzy TOPSIS methods to software requirements selection. Alex. Eng. J. 61, 10851–10870.
Nogarotto, A., 2018. Mapping the bedrock K_2O, U and Th concentration in Italy - Towards the European Atlas of Natural Radiation. Master's thesis, Alma Mater Studiorum. University of Bologna. http://amslaurea.unibo.it/15754/.
Panagos, P., Meusburger, K., Alewell, C., Montanarella, L., 2012. Soil erodibility estimation using LUCAS point survey data of Europe. Environ. Model. Softw. 30, 143–145. https://doi.org/10.1016/j.envsoft.2011.11.002.
Panagos, P., Meusburger, K., Ballabio, C., Borrelli, P., Alewell, C., 2014. Soil erodibility in Europe: a high-resolution dataset based on LUCAS. Sci. Total Environ. 479–480, 189–200.
Panagos, P., Van Liedekerke, M., Borrelli, P., Köninger, J., Ballabio, C., Orgiazzi, A., Lugato, E., Liakos, L., Hervas, J., Jones, A., Montanarella, L., 2022. European Soil Data Centre 2.0: Soil data and knowledge in support of the EU policies. Eur. J. Soil Sci. 73 (6). https://doi.org/10.1111/ejss.13315.
Parsa, M., Maghsoudi, A., Yousefi, M., Sadeghi, M., 2016. Prospectivity modeling of porphyry-Cu deposits by identification and integration of efficient mono-elemental geochemical signatures. J. Afr. Earth Sci. 114, 228–241.
Pazand, K., Hezarkhani, A., Ataei, M., 2012. Using TOPSIS approaches for predictive porphyry Cu potential mapping: a case study in Ahar-Arasbaran area (NW, Iran). Comput. Geosci. 49, 62–71.
Pereira, A.J.S.C., Godinho, M.M., Neves, L.J.P.F., 2010. On the influence of faulting on small-scale soil-gas radon variability: a case study in the Iberian Uranium Province. J. Environ. Radioact. 101, 875–882.
Petermann, E., Bossew, P., 2021. Mapping indoor radon hazard in Germany: the geogenic component. Sci. Total Environ. 780, 146601.
Petermann, E., Meyer, H., Nussbaum, M., Bossew, P., 2021. Mapping the geogenic radon potential for Germany by machine learning. Sci. Total Environ. 754, 142291.
Raines, G.L., Sawatzky, D.L., Bonham-Carter, G., 2010. New ArcGIS 10 in fuzzy logic tools [Online]. https://api.semanticscholar.org/CorpusID:35841592.
Saaty, T.L., 1977. A scaling method for priorities in hierarchical structures. J. Math. Psychol. 15, 234–281.
Saaty, T.L., Vargas, L.G., 2013. The Analytic Network Process. In: Decision Making with the Analytic Network Process. In: International Series in Operations Research Management Science, 195. Springer, Boston, MA. https://doi.org/10.1007/978-1-4614-7279-7_1.
Sakoda, A., Ishimori, Y., Yamaoka, K., 2011. A comprehensive review of radon emanation measurements for mineral, rock, soil, mill tailing and fly ash. Appl. Radiat. Isot. 69, 1422–1435.
Seminsky, K.Zh., Bobrov, A.A., Demberel, S., 2014. Variations in radon activity in the crustal fault zones: spatial characteristics. Izv. Phys. Solid Earth 50, 795–813.
Shih, H.-S., Shyur, H.-J., Lee, E.S., 2007. An extension of TOPSIS for group decision making. Math. Comput. Model. 45 (7–8), 801–813.
Singh, V., Kumar, V., Singh, V.B., 2023. A hybrid novel fuzzy AHP-TOPSIS technique for selecting parameter-influencing testing in software development. Decis. Anal. J. 6, 100159.
Smethurst, M.A., Watson, R.J., Baranwal, V.C., Rudjord, A.L., Finne, I., 2017. The predictive power of airborne gamma ray survey data on the locations of domestic radon hazards in Norway: a strong case for utilizing airborne data in large-scale radon potential mapping. J. Environ. Radioact. 166, 321–340.
Tavana, M., Hatami-Marbini, A., 2011. A group AHP-TOPSIS framework for human spaceflight mission planning at NASA. Expert Syst. Appl. 38 (11), 13588–13603. https://doi.org/10.1016/j.eswa.2011.04.108.
Timkova, J., Fojtikova, I., Pacherova, P., 2017. Bagged neural network model for prediction of the mean indoor radon concentration in the municipalities in Czech Republic. J. Environ. Radioact. 166, 398–402.
Tozzi, M., Kissel, C., Funiciello, R., Laj, C., Parotto, M., 1988. A clockwise rotation of southern Apulia? Geophys. Res. Lett. 15, 681–684.
UNSCEAR (The United Nations Scientific Committee on the Effects of Atomic Radiation), 1982. United Nations Ionizing Radiation, Sources and Biological Effects. Report to the General Assembly, with annexes, United Nations, New York.
Viel, M., Damiani, V., Setti, M., 1986. Particle size characteristics and mineralogical composition of the sediments of the Apulian shelf. In: Environmental Survey of the Coastal Marine System of the Apulia Region, pp. 127–148.
Ying, H., 2003. A general technique for deriving analytical structure of fuzzy controllers using arbitrary trapezoidal input fuzzy sets and Zadeh AND operator. Automatica 39, 1171–1184.
Yousefi, M., Carranza, E.J.M., 2015. Geometric average of spatial evidence data layers: a GIS-based multi-criteria decision-making approach to mineral prospectivity mapping. Comput. Geosci. 83, 72–79.
Zadeh, L.A., 1965. Fuzzy sets. Inf. Control. 8 (3), 338–353.
Zhang, J., Su, Y., Wu, J., Liang, H., 2015. GIS based land suitability assessment for tobacco production using AHP and fuzzy set in Shandong province of China. Comput. Electron. Agric. 114, 202–211.
Zimmermann, H.-J., Zysno, P., 1980. Latent connectives in human decision making. Fuzzy Sets Syst. 4, 37–51.